Lateral gene transfer drives metabolic flexibility in the anaerobic methane oxidising archaeal family *Methanoperedenaceae*

Andy O. Leu[a], Simon J. McIlroy[a], Jun Ye[a], Donovan H. Parks[a], Victoria J. Orphan[b], Gene W. Tyson[a,#]

[a]Australian Centre for Ecogenomics, School of Chemistry and Molecular Biosciences, University of Queensland, Brisbane, Australia

[b]Department of Geological and Planetary Sciences, California Institute of Technology, Pasadena, CA 91106, USA

Running Head: Metabolic diversity of the *Methanoperedenaceae*

Address correspondence to: Gene W. Tyson, g.tyson@uq.edu.au.

Andy O. Leu and Simon J. McIlroy contributed equally to this work. Author order reflects the order in which the authors joined the project.

Abstract word count: 246

Article word count: 5216

Abstract

Anaerobic oxidation of methane (AOM) is an important biological process responsible for controlling the flux of methane into the atmosphere. Members of the archaeal family *Methanoperedenaceae* (formerly ANME-2d) have been demonstrated to couple AOM to the reduction of nitrate, iron, and manganese. Here, comparative genomic analysis of 16 *Methanoperedenaceace* metagenome-assembled genomes (MAGs), recovered from diverse environments, revealed novel respiratory strategies acquired through lateral gene transfer (LGT) events from diverse archaea and bacteria. Comprehensive phylogenetic analyses suggests that LGT has allowed members of the *Methanoperedenaceae* to acquire genes for the oxidation of hydrogen and formate, and the reduction of arsenate, selenate and elemental sulfur. Numerous membrane-bound multi-heme *c* type cytochrome complexes also appear to have been laterally acquired, which may be involved in the direct transfer of electrons to metal oxides, humics and syntrophic partners.

Importance

AOM by microorganisms limits the atmospheric release of the potent greenhouse gas methane and has consequent importance to the global carbon cycle and climate change modelling. While the oxidation of methane coupled to sulphate by consortia of anaerobic methanotrophic (ANME) archaea and bacteria is well documented, several other potential electron acceptors have also been reported to support AOM. In this study we identify a number of novel respiratory strategies that appear to have been laterally acquired by members of the *Methanoperedenaceae* as they are absent in related archaea and other ANME lineages. Expanding the known metabolic potential for members of the *Methanoperedenaceae*

provides important insight into their ecology and suggests their role in linking methane oxidation to several global biogeochemical cycles.

Introduction

Anaerobic oxidation of methane (AOM) is an important microbiological process moderating the release of methane from anoxic waters and sediments into the atmosphere (1-4). Several diverse uncultured microbial lineages have been demonstrated to facilitate AOM. The bacterium "*Candidatus* Methylomirabilis oxyfera" is proposed to couple AOM to denitrification from nitrite, generating oxygen from nitric oxide for the activation of methane (5). Different lineages of anaerobic methanotrophic (ANME) archaea are hypothesised to mediate AOM through the reversal of the methanogenesis pathway and conserve energy using mechanisms similar to those found in methylotrophic and aceticlastic methanogens (6). Unlike methanogens, most of these ANMEs encode a large repertoire of multi-heme *c*-type cytochromes (MHCs), which are proposed to mediate direct interspecies electron transfer to syntrophic sulfate-reducing bacteria (SRB)(7, 8), and/or the reduction of metal oxides and humic acids (9-12).

Currently, several clades within the archaeal phylum Euryarchaeota have been shown to be capable of anaerobic methanotrophy and include ANME-1a-b, ANME-2a-c, *Methanoperedenaceae* (formerly known as ANME-2d), and ANME-3 (refs. 13, 14, 15). Marine ANME lineages are often observed to form consortia with SRBs, with ANME-1 and ANME-2 (a,b, and c) being associated with multiple genera within Desulfobacterales and *Desulfobulbaceae* (13, 16-20), thermophilic ANME-1 with "*Candidatus* Desulfofervidus auxilii" (8, 21) and ANME-3 with SRBs of the *Desulfobulbus* (22). While members of the family *Methanoperedenaceae* have also recently been associated with SRB of the family

Desulfobulbaceae in a freshwater lake sediment (23), they also appear to oxidise methane independently using a range of electron acceptors. The type species of this family, "*Candidatus* Methanoperedens nitroreducens", was originally enriched in a bioreactor and shown to couple AOM to the reduction of nitrate via a laterally transferred nitrate reductase (15). Subsequently, "*Ca.* Methanoperedens sp. BLZ1" was also found to encode a laterally transferred nitrite reductase, which is also present in the genome of "*Ca.* M nitroreducens", potentially allowing these microorganisms to coupled AOM to dissimilatory nitrate reduction to ammonia (DNRA) (24). More recently, three novel species belonging to the *Methanoperedenaceae* were enriched in bioreactors demonstrated to couple AOM to the reduction of insoluble iron or manganese oxides (9, 12). These microorganisms did not encode dissimilatory nitrate reduction pathways, but instead were inferred to use multiple unique MHCs during metal-dependent AOM to facilitate the transfer of electrons to the metal oxides (9, 12), consistent with the extracellular electron transfer mechanisms proposed for marine ANME (7, 8). Bioreactor performance and 16S rRNA gene amplicon data has also been used to suggest that members of the *Methanoperedenaceae* are capable of AOM coupled to the reduction of selenate and chromium(VI), although this remains to be confirmed with more direct evidence (25, 26). Notably, members of the *Methanoperedenaceae* have been observed to facilitate AOM coupled to multiple terminal electron acceptors within the same natural sediment (27). Individual members of the family can possess such metabolic flexibility, with a lab-enriched species shown to couple AOM to the reduction of nitrate, iron and manganese oxides (10). Given the relatively poor genomic representation of the *Methanoperedenaceae*, and the lack of detailed physiological studies of its members, it is likely that considerable metabolic diversity for the lineage remains to be discovered.

In this study, comparative analysis was conducted on 16 *Methanoperedenaceae* metagenome-assembled genomes (MAGs) recovered from various environments to investigate the metabolic diversity and versatility of the family and to understand the evolutionary mechanisms responsible for these adaptations. These analyses indicate that members of the *Methanoperedenaceae* have acquired a large number of genes through LGT that potentially allow AOM to be coupled to a wide range of electron acceptors, suggesting their role in methane oxidation extends beyond environments with nitrate and metal oxides.

Results and Discussion

Expanding the genomic representation of the Methanoperedenaceae

In order to explore the metabolic diversity within the *Methanoperedenaceae,* comparative genomic analysis was performed on both publicly available and newly acquired MAGs (**Table 1**). The publicly available genomes include five MAGs recovered from bioreactors where AOM is coupled to the reduction of nitrate ("*Ca.* Methanoperedens nitroreducens"; M.Nitro (15), and "*Ca.* Methanoperedens sp. BLZ2"; BLZ2 (ref. 28)), iron ("*Ca.* Methanoperedens ferrireducens"; M.Ferri (9)) and manganese ("*Ca.* Methanoperedens manganicus" and "*Ca.* Methanoperedens manganireducens", Mn-1 and Mn-2, respectively (12)). Also included are two environmental MAGs recovered from groundwater samples from the Horonobe and Mizunami underground research laboratories in Japan (HGW-1 and MGW-1) (29, 30), and one MAG from an Italian paddy soil sample (IPS-1) (31). In order to recover additional genomes belonging to the family, GraftM (32) was used to screen public metagenome sequence datasets from NCBI for *Methanoperedenaceae*-related 16S rRNA and *mcrA* gene sequences. Subsequent assembly and genome binning on datasets found to contain *Methanoperedenaceae*-like sequences led to the recovery of an additional eight MAGs

112 belonging to the family. Six of these were from arsenic contaminated groundwater samples
113 (ASW-1-6), and a further two from sediment and groundwater samples from a copper mine
114 tailings dam (CMD-1 and CMD-2). All 16 MAGs are highly complete (≥87.4%) with low
115 contamination (≤5.9%) based on 228 Euryarchaeota-specific marker genes (**Table 1**)(33).
116 These genomes vary in GC content from 40.2 to 50.7% and range in size from 1.45 to 3.74
117 Mbp.

118 A genome tree including 1,199 publicly available archaeal genomes, based on a concatenated
119 set of 122 marker genes (34), confirmed the phylogenetic placement of the 16 MAGs within
120 the *Methanoperedenacae*. The genome tree supports that these MAGs form a monophyletic
121 clade sister to the GoM-Arc1 genomes (**Figure 1**). These genomes likely represent three
122 separate genera within the family, based on their placement within a reference tree, relative
123 evolutionary distance, FastANI distance, and average amino acid identity (AAI (35); 61.3 to
124 89.2%; **Figure S1**). All MAGs were classified as members of the genus "*Ca*.
125 Methanoperedens", except HGW-1 and ASW-3 which appear to represent independent genus
126 level lineages (**Figure 1**). Phylogenetic analysis of the six MAGs containing 16S rRNA genes
127 was consistent with the genome tree (**Figure S2**), supporting their classification as members
128 of the *Methanoperedenaceae* family.

129

130 *Potential electron donors used by the Methanoperedenaceae*
131 Metabolic reconstruction of the *Methanoperedenaceae* MAGs showed that all genomes
132 encoded the central methanogenesis pathway, inclusive of the methyl-coenzyme M reductase,
133 supporting their potential for the complete oxidation of methane to CO_2 (**Figures 2 and S3**).
134 The annotation of membrane-bound formate dehydrogenases (FdhAB) in five of the
135 *Methanoperedenaceae* MAGs (Mn-2, ASW-4, ASW-1, MGW-1, and BGW-1; **Figure 3**)

suggests that some members of the family may also oxidise formate (E_0 [CO_2/$HCOO^-$] = −430 mV) (36). As the enzyme is reversible, these species could also potentially produce formate as a supplementary electron sink during AOM. Formate was suggested as a putative electron shuttle between ANME-1 and their syntrophic partner SRB, based on the annotation and expression of an *fdhAB* in ANME-1, but this has not been supported with physiological studies (37, 38). The putative formate dehydrogenase encoded in the Mn-2 MAG is phylogenetically related to an FdhA found in the genome of *Caldiarchaeum subterraneum*, while those encoded by ASW-4, ASW-1, MGW-1, and BGW-1 appear to be more similar to the FdhA of *Methanocellaceae* archaeon UBA148 (**Figure 3**).

The use of hydrogen (H_2; E_0 = -414mV (39)) as an electron source was previously suggested for MGW-1 and HGW-1 which encode Group 1 membrane-bound NiFe hydrogenase complexes, composed of a NiFe catalytic subunit, a FeS electron transfer subunit, and a membrane-bound *b*-type cytochrome (29, 30). These hydrogenases, along with similar Group 1 NiFe hydrogenases identified in the ASW-6 and CMD-2 MAGs, form a monophyletic clade with those encoded by the MAG for "*Ca.* Hydrothermarchaeota" (JdFR-18), which belongs to the archaeal phylum Hydrothermarchaeota (40), and several members of the Halobacterota (**Figure S4A**). The ASW-3 and ASW-5 MAGs encode Group 1 NiFe hydrogenases that are basal to Vho/Vht/Vhx hydrogenases encoded by members of the genus *Methanosarcina* (41). As the ASW-5 NiFe hydrogenase does not encode a *b*-type cytochrome (**Figure S4B**), it is unclear how electrons are derived from hydrogen. In addition to the membrane-bound NiFe hydrogenases, the M.Nitro MAG was found to encode genes for two different sets of Group 3b cytoplasmic hydrogenases (**Figure S4A**). The MGW-1 (ref. 29) and ASW-2 MAGs also encode Group 3b hydrogenases which have been implicated in hydrogen evolution and nicotinamide adenine dinucleotide phosphate (NADPH) reduction (42). Similar complexes have also been shown to have hydrogen oxidation and elemental sulfur reducing capabilities

(42-44). It is unknown how these Group 3b hydrogenases would contribute to energy conservation given their predicted cytoplasmic localisation. The functionality of the annotated Group 1 and 3 NiFe hydrogenases is supported by the identification of the NiFe binding motifs (L1 and L2) on their NiFe catalytic subunits and the annotation of all or most of the hydrogenase maturation genes (hypA-F) on the same *Methanoperedenaceae* MAGs (**Dataset S1D**). The potential for some *Methanoperedenceae* to couple the oxidation of hydrogen and/or formate to the reduction of exogenous electron acceptors would be advantageous with the dynamic availability of methane in natural environments (45).

Pathways for energy conservation during AOM in the Methanoperedenaceae

All members of the *Methanoperedenaceae* encode the Fpo complex (FpoABCDHIJ$_1$J$_2$LMNOF), a homolog of Complex I (nuoABCDEFGHIJKLMN), which is hypothesised to oxidize $F_{420}H_2$ coupled to the reduction of a membrane-bound soluble electron carrier, and translocation of two protons out of the cell (**Figures 2 and S5A**) (41, 46). While members of the *Methanosarcinales* and marine ANME-2a are reported to typically use methanophenazine (MP) as their membrane-bound soluble electron carrier, the *Methanoperedenaceae* and ANME-1 have previously been suggested to use menaquinone (MK) based on the annotation of the futalosine pathway for MK biosynthesis in several MAGs representing these lineages (47). Comparative genomic analysis of the 16 *Methanoperedenaceae* MAGs revealed that the futalosine pathway is a conserved feature of all members, except the most basal member ASW-3 (see later; **Dataset S1A**). As has previously been suggested by Arshad *et al.*, (48), the larger difference in redox potential between F_{420} (E_0 = -360mV) and MK (E_0 = -80mV (49)), relative to F_{420} and MP (E_0 = -165mV (50)), would theoretically allow the Fpo complex to translocate more protons

($3H^+/2e^-$) out of the cell for every molecule of F_{420} oxidised, giving a higher overall energetic yield from AOM (**Figure S5B**).

Phylogenetic analysis of the Fpo complex in the *Methanoperedenaceae* MAGs showed that the FpoKLMNO subunits are homologous to proteins found in MP utilising members of the *Methanosarcinales*. The FpoABCDHIJ$_1$J$_2$ subunits are more similar to those found in microorganisms known to use MK and other quinones, which have more positive redox potentials (**Figures S5 and S6**; **Dataset S1E**) (51). As the latter subunits (specifically FpoH) are responsible for interaction with the membrane soluble electron carrier pool (52, 53), this observation provides further support to the use of MK by members of the *Methanoperedenaceae*. To our knowledge, this is the first reported example of a lineage encoding a 'hybrid' Complex I homolog possessing subunits with homology to those found in phylogenetically diverse microorganisms (**Figure S6**). The GoM-Arc-I MAGs appear to possess the MK biosynthesis pathway and a similar 'hybrid' Fpo complex to the *Methanoperedenaceae* (**Figure S6**), suggesting that the evolutionary adaptation of the lineage to utilise MK occurred prior to the divergence of these two related families. Members of the GoM-Arc-1 clade possess Mcr-like complexes (**Figure S3**) and are suggested to use short-chain alkanes – possibly ethane (54, 55). Interestingly, the FpoMNO subunits of the ASW-3 MAG cluster with those of the other members of the *Methanoperedenaceae* family, while their FpoABCDHIJ$_1$J$_2$KL subunits are most similar to those of the ANME-2a and other members of the *Methanosarcinales* (**Figure S6**). While the genes involved in MP biosynthesis are not known, the absence of the MK biosynthesis pathway indicate that ASW-3 likely uses MP. As the most basal lineage of this family, ASW-3 may have adapted to use MP after the evolutionary divergence of the GoM-Arc-I and *Methanoperedenaceae*, although further genomic representation of this lineage is required to verify this hypothesis.

Comparative genomic analyses of the *Methanoperedenaceae* MAGs revealed that none of these genomes encode an Rnf complex, which is hypothesised to re-oxidise ferredoxin coupled to the transport of sodium ions out of the cell and the reduction of MP in marine ANME-2a (7, 56) and other methylotrophic methanogens (41, 57, 58). In the absence of this complex, ferredoxins could be re-oxidised with a 'truncated' Fpo complex, similar to the Fpo complex possessed by *Methanosaeta thermophila* (59). Alternatively an electron confurcating mechanism could be used for the re-oxidation of ferredoxin, coenzyme M, and coenzyme B, coupled to the reduction of two F_{420} via a cytoplasmic complex composed of a heterodisulfide reductase (HdrABC) and a F_{420} hydrogenase subunit B (FrhB) (24). The two additional $F_{420}H_2$ could subsequently be fed back into the Fpo complex, greatly increasing the overall bioenergetic yield (24) (**Figure 2**). All of the *Methanoperedenaceae* MAGs have the genetic potential for these alternate strategies for re-oxidation of ferredoxin during AOM, however, further experimental validation is required to test these hypotheses.

Conservation of unique menaquinone: cytochrome c oxidoreductases within the Methanoperedenaceae

Five different putative MK:cytochrome c oxidoreductase gene clusters (**Figures 1 and 2**; **Dataset S1A**) that are hypothesised to mediate the transfer of electrons out of the cytoplasmic membrane were identified in the *Methanoperedenaceae* MAGs. These gene clusters include a non-canonical bc1/b6f complex adjacent to two hypothetical proteins and two 6-haem multi-heme cytochromes (MHCs; Group 1), two clusters where a *b*-type cytochrome is adjacent to a 6-haem MHC (Groups 2 and 3), and another two clusters where a NrfD-like transmembrane protein is adjacent to an electron transferring 4Fe-4S ferredoxin iron-sulfur protein and MHCs (Groups 4 and 5; **Figure 2**). These bc and NrfD complexes are frequently found in

other metal reducing microorganisms and mediate electron transport from the cytoplasm to the periplasm (60-62).

Most of the 16 *Methanoperedenaceae* MAGs (except CMD-1 and ASW-3) have more than one of these MK:cytochrome oxidoreductase complexes and 11 have at least four (**Figure 1**). ASW-3 is the only MAG not to encode any MK: cytochrome *c* oxidoreductases, which is consistent with its putative use of MP. A gene encoding a cytochrome-*b* found to be most similar to "*Ca.* Methanohalarchaeum thermophilum" was identified in ASW-3; however, in the absence of a collocated MHC gene, the extracellular electron transfer step for this microorganism is unclear.

Phylogenetic analysis of the membrane-bound subunits of the MK:cytochrome *c* oxidoreductases (**Figure 2**), which include the NrfD subunits (from Groups 1 and 2) and the *b*-type cytochromes (from Groups 3, 4 and 5), showed that they have been potentially laterally transferred from diverse donors (**Figure S7**). The *Methanoperedenaceae* NrfD subunits formed independent clusters with sequences from members of the Dehalococcoidales family RBG-16-60-22 (Group 1) and a single MAG (RBG-16-55-9) from the candidate phylum Bipolaricaulota (Group 2; **Figure S7A**). The *b*-type cytochromes of the *Methanoperedenaceae* belong to three distinct clades (**Figure S7B**). The *b*-type cytochromes from Groups 3 and 4 clustered with proteins from GoM-ArcI, indicating vertical genetic inheritance from an ancestor of these two families, and Group 5 proteins clustered with those from the class Archaeoglobi (40).

The conservation of multiple conserved laterally transferred MK:cytochrome *c* oxidoreductases in most of the *Methanoperedenaceae* MAGs may contribute to the reported ability for members of the family to reduce a variety of electron acceptors with a range of redox potentials that include Fe(III) oxide reduction (-100mV to 100mV) (63), nitrate

(+433mV)(24), and Mn(IV) (+380mV) (36). Transcriptomic analyses has shown that different MK:cytochrome *c* oxidoreductases are expressed in different species of the genus "*Ca*. Methanoperedens" during AOM coupled to the reduction of Fe(III) oxides (9), Mn(IV) oxides (12), and nitrate (15, 24). A similar phenomenon is observed for the species *Geobacter sulfurreducens*, where different extracellular electron pathways were used when reducing different electron acceptors (64).

Potential electron acceptors used by the Methanoperedenaceae

Annotation of the *Methanoperedenaceae* MAGs revealed a wide array of genes associated with previously undescribed respiratory strategies for the family that appear to have been acquired via LGT. Principally, these are putative terminal oxidoreductase complexes belonging to the Complex-Iron-Sulfur-Molybdenum (CISM) superfamily that were absent in the genomes of related archaeal lineages (**Figure 3**). These complexes are composed of a catalytic subunit, an iron-sulfur protein, and a membrane-bound subunit, and facilitate the transfer of electrons between the electron acceptor/donor and the MK pool (**Figure 2**).

As previously reported, the MAGs M.Nitro, BLZ2, and IPS-1 encode respiratory nitrate reductases that are part of the CISM superfamily, allowing them to independently mediate AOM coupled to nitrate reduction (15, 24, 65). Based on phylogenetic analysis (**Figure 3**), genes encoding cytoplasmic nitrite oxidoreductases (NxrA) were identified in the IPS-1, BLZ2, and M.Nitro MAGs, and a nitrate reductase closely related to NarG proteins was identified in the BLZ2 MAG. Of the *Methanoperedenaceae* MAGs, only the M.Nitro and BLZ2 MAGs possess a putative nitrite reductase (NrfA) for DNRA. The M.Ferri MAG encodes an assimilatory nitrate reductase (NarB/NasA) most similar to a protein encoded by the *Magnetobacterium casensis* (**Figure 3**). However, in the absence of an annotated nitrite

reductase in the M.Ferri MAG, the potential of this microorganism for assimilatory nitrate reduction is unclear.

Multiple MAGs (ASW-2,3,5,6, and Mn-2) were also found to encode putative selenate reductases (SrdA; **Figure 3**), suggesting their ability for Se(VI)-dependent AOM. Recently, a bioreactor enrichment of a member of the genus "*Ca.* Methanoperedens" exhibited AOM activity when nitrate was substituted with selenate (26). However, as no meta-omic analyses was conducted for the community, it is unclear if the dominant "*Ca.* Methanoperedens" possessed a putative selenate reductase, or if it was directly responsible for the observed selenate reduction.

The ASW-1 and ASW-3 MAGs encode a putative sulfur reductase (SreABC). This annotation is supported by its phylogenetic clustering of the catalytic sub-unit with SreA from *Aquifex aeolicus* (**Figure 3**), which has been shown to reduce elemental sulfur, as well as tetrathionate and polysulfide (66). This is the first genomic evidence suggesting that members of the *Methanoperedenaceae* may be involved in respiratory sulfur-dependent AOM and warrants further investigation. ANME-1 have been proposed to couple AOM to the reduction of polysulfide in a biogenic hydrocarbon seep sediment, but this was based on the annotation and high expression of a putative sulfide: quinone oxidoreductase (SQR)(67). Genes for dissimilatory sulfate reduction pathways were absent in the *Methanoperedenaceae* MAGs, consistent with other ANME lineages (68). MGW-1 was recently speculated to directly couple AOM to sulfate reduction utilising assimilatory sulfate reduction pathways. This hypothesis was based on the lack of large MHCs or identifiable alternate electron acceptor complexes encoded in the MAG (29). Several of the *Methanoperedenaceae* MAGs, and those of other ANME lineages, contain candidate genes associated with assimilatory sulfate reduction, but a dissimilatory role for these has not been shown (68).

The M.Nitro MAG encodes two putative reductases belonging to the arsenate reductase (ArrA) and arsenite oxidase (ArxA) group (**Figure 3**). The BLZ2, ASW-1, ASW-4, IPS-1 MAGs also encode reductases that cluster with the M.Nitro ArxA-like sequence. The ArxA protein has been found to be capable of both arsenite oxidation and arsenate reduction (69), which would allow the *Methanoperedenaceae* possessing these ArxA-like proteins to utilise arsenate as a terminal electron acceptor. Proteins encoded by the ASW-3 and "*Candidatus* Acetothermum autotrophicum" (70) (**Figure 3**) form a deep branching clade adjacent to the ArxA and ArrA groups, suggesting these species might also have the potential to respire on arsenic compounds. It is noteworthy that the ASW-1, 3, and 4 MAGs were recovered from a Bangladesh arsenic contaminated groundwater sample (**Table 1**), indicating a role for LGT in their niche-specific adaptation. The possibility of AOM coupled to arsenate (As(V)) reduction has important environmental implications given the wide distribution of arsenic in nature, including subsurface drinking water aquifers (71), and the toxicity and mobility of its reduced form, arsenite (As(III)) (72) (73). Arsenic reduction and mobilisation has been linked to an inflow of organic carbon in contaminated aquifers where methane (~1mM) and arsenate co-occur (74, 75).

Additional putative oxidoreductases clades that are not closely associated with any well characterised CISM proteins were also found in the *Methanoperedenaceae* MAGs. This includes two proteins encoded by the ASW-3 and ASW-6 MAGs that cluster with a protein of unknown function from a *Brocadiales* MAG (76), and the CMD-1 protein that clusters with a protein from *Brocadia fulgida*, an ammonium oxidising and nitrite reducing microorganism (77). In general, given the large range of substrates utilized by the CISM superfamily and the few biochemically characterized proteins, the predicted function of all those annotated in the *Methanoperedenaceae* require empirical verification. Nonetheless, the

range of putative CISM superfamily proteins encoded by members of the family likely indicates diverse respiratory strategies that remain to be characterised.

The diversity of the MHCs in the Methanoperedenaceae

Members of the *Methanoperedenaceae* possess a diverse repertoire of MHCs which have been suggested to facilitate the transfer of electrons from the re-oxidation of MK to metal oxides (9, 10, 78) or direct interspecies electron transfer (DIET) to a syntrophic partner. Analyses of the *Methanoperedenaceae* revealed that they possess between three (MGW-1) and 49 (IPS-1) MHCs (containing at least three CXXCH motifs) with an average of 26 – the highest average of any archaeal family (**Dataset S1F and S1G**). Notably, relatively high numbers of MHCs per genome are almost exclusively found in microorganisms associated with DIET, metal and/or sulfur reduction, such as the *Geobacteraceae* (79) (≤ 87 MHCs), *Shewanellaceae* (80) (≤ 63 MHCs), *Desulfurivibrionaceae* (20), *Desulfuromonadaceae* (20) and *Defferisomataceae* (81) (≤ 50 MHCs; **Dataset S1G**). Interestingly, seven of the 16 members of the *Methanoperedenaceae* encode MHCs with more than 50 heme binding sites (ASW-5, ASW-6, BLZ2, HGW-1, M. ferri, Mn-1 and Mn-2), with the 113 heme MHC encoded by Mn-2 the largest identified in any microorganism (**Dataset S1F**).

The 414 putative MHCs identified in the *Methanoperedenaceae* MAGs clustered into 82 orthologous protein families (**Figure S8**). Only one protein family (OG0000252) included at least one MHC from each member, which suggests low conservation of these genes within the *Methanoperedenaceae*. Out of the 82 MHC protein families, 14 were identified in at least eight of the 16 MAGs, with five of these found within the conserved MK:cytochrome *c* oxidoreductase clusters. A lack of conservation of MHCs is also observed for the anaerobic metal-respiring genus *Geobacter*, where 14% of the MHCs encoded in six analysed genomes

were found to be conserved (61). Thirty-nine of the 82 MHC protein families had significant hits (1e-20, ≥50% AAI) to homologs from diverse lineages across the bacterial and archaeal domains in the GTDB89 database, indicating potential LGT of these genes (**Figure S9**). These lineages notably included the metal reducing *Geobacteraceae* and *Shewanellaceae*, along with the alkane oxidising *Archaeoglobaceae*, Methylomirabilota (NC10), and other ANME-lineages (**Figure S9**).

Putative function of MHCs in the Methanoperedenaceae

Very few of the *Methanoperedenaceae* MHCs could be associated with a specific function. Two orthologous groups were annotated as nitrite: ammonium oxidoreductases (NrfA) with homologs identified in bacterial MAGs classified to the Anaerolineales (OG0004545; ≥66.3% AAI) and the candidate phylum UBP4 (OG0012490, 64.56% AAI). Several MHCs were also identified as part of the MK:cytochrome *c* oxidoreductase clusters, with homologs observed in members of the archaeal family *Archaeaglobaceae* (OG001557, OG000137, OG0001550, ≥57.3% AAI; **Figure S9**). MHC/S-layer fusion proteins were suggested to mediate the transfer of electrons across the S-layer for marine ANME-2 (ref. 7) and were relatively highly expressed by '*Ca.* M. manganicus' and '*Ca.* M. manganireducens' during AOM coupled to Mn(IV) reduction (12). Conversely, only low expression of MHC/S-layer protein genes encoded by '*Ca.* M. ferrireducens' was observed during AOM coupled to Fe(III) reduction (9). In addition, despite all the *Methanoperedenaceae* MAGs containing S-layer proteins, five do not encode MHC proteins with an S-layer domain (ASW-3, CMD-1, CMD-2, HGW-1 and MGW-1), indicating alternative mechanisms for electron transfer across the S-layer to extracellular MHCs for these species.

Predicted extracellular MHCs are hypothesized to facilitate the final transfer of electrons from the *Methanoperedenaceae* to metal oxides (9). Interestingly, '*Ca.* M. manganicus' and '*Ca.* M. manganireducens' showed differential expression patterns in the complement of shared extracellular MHCs during AOM coupled to Mn(IV) reduction. In addition, no orthologs for the two MHCs highly transcribed by '*Ca*. M. ferrireducens' during AOM coupled to Fe(III) reduction (9) were identified in other members of the *Methanoperedenaceae* (OG0011636 and OG0003254; **Figure S8**), suggesting that BLZ2 utilises a different MHC for iron reduction linked to AOM (10). These observations suggest that the *Methanoperedenaceae* can utilise multiple mechanisms for the reduction of similar metal oxides. Differential expression of conserved MHCs linked to extracellular electron transfer was also observed for different *Geobacteraceae* species enriched on electrodes when exposed to the same surface redox potential (82). As suggested for members of the *Geobacteraceae*, the large MHC repertoire possessed by the *Methanoperedenaceae* may enable adaptation to the use of a range of terminal electron acceptors.

This study has substantially improved the genome coverage of the *Methanoperedenaceae*. Comparative genomic analysis of this lineage highlights a metabolic plasticity not found in other ANME clades. The subsequent ability of members of the family to adapt to the use of terminal electron acceptors across a range of redox potentials likely contributes to their success in diverse environments (**Table 1**). Notably, based on the genome tree (**Figure 1**), and the lack of conservation of MHCs (**Figure S8**), the acquisition of these genes is not congruent with the genome-based phylogeny of the family, suggesting niche specific adaptations as the main driver for these LGT events. While further studies are necessary to verify the general physiology and energy conservation mechanisms of the *Methanoperedenaceae* in different environments, this study provides genomic evidence that members of the family may play key roles in coupling cycling of carbon with selenate, sulfur,

and arsenic in addition to nitrogen and metal oxides. Continued sequencing and characterisation of this lineage will reveal the full extent of their metabolic versatility and influence on global biogeochemical cycles.

Materials and Methods

Recovery of the genomes from SRA

The NCBI sequence read archive (SRA (83)) was accessed on the 22nd of March 2017 and 14516 datasets classified as environmental metagenomes were downloaded. The metagenomic datasets were screened using GraftM (32) to search for 16S rRNA and *mcrA* gene sequences similar to those from members of the *Methanoperedenaceae*. For datasets where members of the family were detected, all paired-end read sets were trimmed and quality filtered using PEAT v1.2.4 (ref. 84). For genomes, CMD-1 and CMD-2, SRR5161805 and SRR5161795 reads were coassembled using Metaspades, version 3.10.0 using the default parameters (85). For the ASW genomes, SRR1563167, SRR1564103, SRR1573565, and SRR1573578 reads were coassembled using Metaspades, version 3.10.0 with default parameters (85). Mapping of quality reads was performed using BamM v1.7.3 with default parameters (https://github.com/Ecogenomics/BamM). Metagenomic assembled genomes were recovered from the assembled metagenomes using uniteM v0.0.14 (https://github.com/dparks1134/UniteM). The *Methanoperedenaceae* MAGs were further refined by reassembling the mapped quality trimmed reads with SPAdes using the –careful and –trusted-contigs setting. Additional scaffolding and resolving ambiguous bases of the MAGs was performed using the 'roundup' mode of FinishM v0.0.7 (https://github.com/wwood/finishm). Completeness and contamination rates of the population bins were assessed using CheckM v1.0.11 (ref. 33) with the 'lineage wf' command. The

425 genomes assembled in this study have been deposited in NCBI under the accession numbers
426 SAMN10961276- SAMN10961283.

427

428 *Functional annotation*

429 For all MAGs, open reading frames (ORF) were called and annotated using Prokka v.1.12
430 (ref. 86). Additional annotation was performed using the blastp 'verysensitive' setting in
431 Diamond v0.9.18 (https://github.com/bbuchfink/diamond.git) against UniRef100 (accessed
432 September 2017) (87), clusters of orthologous groups (COG) (88), Pfam 31 (ref. 89) and
433 TIGRfam (Release: January 2014) (90). ORFs were also diamond blastp searched against
434 Uniref100 (accessed September 2017) containing proteins with KO ID. The top hit for each
435 gene with an e-value $<1e^{-3}$ was mapped to the KO database (91) using the Uniprot ID
436 mapping files. Genes of interest were further verified using NCBI's conserved domain search
437 to identify conserved motif(s) present within the gene (92). Psortb v3.0 (ref. 93) was used to
438 predict subcellular localisation of the putative proteins. Pred-Tat was used to predict putative
439 signal peptides (94). Putative multi-heme *c*-type cytochromes (MHCs) were identified by
440 ORFs possessing ≥3 CXXCH motifs. Putative MHCs were subsequently searched for
441 cytochrome *c*-type protein domains using hmmsearch (HMMER v.3.1) (95) with PfamA (96).

442

443 *Construction of genome trees*

444 The archaeal genome tree was constructed using GTDB-Tk (GTDBtk v0.2.2,
445 https://github.com/Ecogenomics/GTDBTk/releases) with a concatenated set of 122 archaeal-
446 specific conserved marker genes inferred from genomes available in NCBI (NCBI RefSeq
447 release 83) (34). Marker genes were identified and aligned in each genome using HMMER
448 v.3.1 (ref. 95), concatenated, and trees were constructed using FastTree V.2.1.8 (ref. 97) with

449 the WAG+GAMMA models. Support values were determined using 100 nonparametric
450 bootstrapping with GenomeTreeTK. The trees were visualised using ARB (98) and formatted
451 using Adobe Illustrator (Adobe, USA).

452

453 *Construction of 16S rRNA gene tree*

454 The 16S rRNA gene was identified in MAGs and used to infer taxonomic assignment of the
455 population genome implementing the SILVA 16S rRNA gene database (Version 132).
456 Sequences were aligned with 426 16S rRNA gene sequences retrieved from the SILVA
457 database using SSU-align v0.1 (ref. 99). The phylogenetic tree was constructed using
458 FastTree V2.1.8 (ref. 97) with the Generalised Time-Reversible and GAMMA model.
459 Support values were determined using 100 nonparametric bootstrapping. The trees were
460 visualised using ARB (98) and formatted using Adobe Illustrator.

461

462 *Calculation of amino acid identity*

463 The *Methanoperedenaceae* MAGs identified in this study were compared to publicly
464 available genomes of the family. Average amino acid identity (AAI) between the genomes
465 was calculated using orthologous genes identified through reciprocal best BLAST hits using
466 compareM v0.0.5 (https://github.com/dparks1134/CompareM).

467

468 *Identification of orthologous proteins*

469 Homologous proteins across all the *Methanoperdenaceae*, GoM-Arc I, ANME-2a, ANME-2c
470 MAGs were identified with OrthoFinder (100) v2.3.3 using default parameters. Gene counts
471 of orthologous groups containing MHCs were used as input for a heatmap using the
472 pheatmap package in R and hierarchical clustering was performed using ward.D2 (ref. 101).

473

474 *Construction of gene trees*

475 Genes of interest in the *Methanoperedenaceae* MAGs were compared against proteins from
476 GTDB v83 database (34) using the genetreetk 'blast' command to identify closely related
477 sequences. For the generation of the gene tree for catalytic subunits of the CISM superfamily,
478 curated protein sequences were also added in the analysis. Accession numbers and amino
479 acid sequences are included in **Dataset S1B**. For the generation of the gene tree for the
480 catalytic subunits of the Group 1 and Group 3 NiFe dehydrogenase, curated sequences from
481 Greening *et al.,* (102) were included in the analysis. Accession numbers and amino acid
482 sequences can be found in **Dataset S1C**. The sequences were subsequently aligned using
483 mafft v7.221 (ref. 103) with the –auto function and the alignment trimmed using trimal v1.2
484 (https://github.com/scapella/trimal) '-automated1' option. A phylogenetic tree was
485 constructed using RAxML v8.2.9 (ref. 104) with the following parameters: raxmlHPC-
486 PTHREADS-SSE3 -T 30 -m PROTGAMMALG -p 12345. Bootstrap values were calculated
487 via non-parametric bootstrapping with 100 replicates. The trees were visualised using ARB
488 (98) or iToL (105) and formatted using Adobe Illustrator (Adobe, USA).

489

490 *Network analysis of MHCs*

491 Putative multi-heme *c*-type cytochromes (MHCs) from GTDB v89 database were identified
492 by ORFs possessing ≥3 CXXCH. Putative MHCs were subsequently searched for
493 cytochrome *c*-type protein domains using hmmsearch (HMMER v.3.1) (95) with PfamA (96).
494 Proteins from each *Methanoperedenaceae* orthogroup were blasted against the GTDB v89
495 MHC protein database using DIAMOND with an evalue cutoff of 1e-20 and ≥50% AAI. The

result was visualised in Cytoscape v3.7.1, removing clusters that contained only, or no, *Methanoperedenaceae* homologs.

Acknowledgements

This work was supported by the Australian Research Council (ARC) (FT170100070) and the U.S. Department of Energy's Office of Biological Environmental Research (DE-SC0016469). AOL was supported by an ARC Australian Postgraduate Award. We thank the AWMC team, particularly Shihu Hu and Zhiguo Yuan, for their ongoing collaboration working on various "*Ca*. Methanoperedens" enrichments.

Competing interests

The authors have nothing to disclose.

References

1. Reeburgh WS. Oceanic methane biogeochemistry. Chemical Reviews. 2007;107(2):486-513.

2. Segarra K, Schubotz F, Samarkin V, Yoshinaga M, Hinrichs K, Joye S. High rates of anaerobic methane oxidation in freshwater wetlands reduce potential atmospheric methane emissions. Nature Communications. 2015;6:7477.

3. Martinez-Cruz K, Sepulveda-Jauregui A, Casper P, Anthony KW, Smemo KA, Thalasso F. Ubiquitous and significant anaerobic oxidation of methane in freshwater lake sediments. Water Research. 2018;144:332-40.

4. Thamdrup B, Steinsdottir HGR, Bertagnolli A, Padilla C, Patin NV, Garcia-Robledo E, et al. Anaerobic methane oxidation is an important sink for methane in the ocean's largest oxygen minimum zone. Limnol Oceanogr. 2019;64(6):2569-85.

5. Ettwig KF, Butler MK, Le Paslier D, Pelletier E, Mangenot S, Kuypers MM, et al. Nitrite-driven anaerobic methane oxidation by oxygenic bacteria. Nature. 2010;464(7288):543-8.

6. McGlynn SE. Energy Metabolism during Anaerobic Methane Oxidation in ANME Archaea. Microbes and Environments. 2017;32(1):5-13.

7. McGlynn SE, Chadwick GL, Kempes CP, Orphan VJ. Single cell activity reveals direct electron transfer in methanotrophic consortia. Nature. 2015;526:531-5.

8. Wegener G, Krukenberg V, Riedel D, Tegetmeyer HE, Boetius A. Intercellular wiring enables electron transfer between methanotrophic archaea and bacteria. Nature. 2015;526(7574):587-90.

9. Cai C, Leu AO, Xie G-J, Guo J, Feng Y, Zhao J-X, et al. A methanotrophic archaeon couples anaerobic oxidation of methane to Fe (III) reduction. The ISME Journal. 2018;12:1929-39.

536 10. Ettwig KF, Zhu B, Speth D, Keltjens JT, Jetten MSM, Kartal B. Archaea catalyze
537 iron-dependent anaerobic oxidation of methane. Proceedings of the National Academy of
538 Sciences. 2016;45:12792-6.
539 11. Scheller S, Yu H, Chadwick GL, McGlynn SE, Orphan VJ. Artificial electron
540 acceptors decouple archaeal methane oxidation from sulfate reduction. Science.
541 2016;351(6274):703-7.
542 12. Leu AO, Cai C, McIlroy SJ, Southam G, Orphan VJ, Yuan Z, et al. Anaerobic
543 methane oxidation coupled to manganese reduction by members of the
544 Methanoperedenaceae. ISME J. 2020;https://doi.org/10.1038/s41396-020-0590-x.
545 13. Knittel K, Lösekann T, Boetius A, Kort R, Amann R. Diversity and distribution of
546 methanotrophic archaea at cold seeps. Applied and Environmental Microbiology.
547 2005;71(1):467-79.
548 14. Orphan VJ, House CH, Hinrichs K-U, McKeegan KD, DeLong EF. Multiple archaeal
549 groups mediate methane oxidation in anoxic cold seep sediments. Proceedings of the
550 National Academy of Sciences. 2002;99(11):7663-8.
551 15. Haroon MF, Hu S, Shi Y, Imelfort M, Keller J, Hugenholtz P, et al. Anaerobic
552 oxidation of methane coupled to nitrate reduction in a novel archaeal lineage. Nature.
553 2013;500(7464):567-70.
554 16. Orphan V, Hinrichs K-U, Ussler W, Paull CK, Taylor L, Sylva SP, et al. Comparative
555 analysis of methane-oxidizing archaea and sulfate-reducing bacteria in anoxic marine
556 sediments. Appl Environ Microbiol. 2001;67(4):1922-34.
557 17. Pernthaler A, Dekas AE, Brown CT, Goffredi SK, Embaye T, Orphan VJ. Diverse
558 syntrophic partnerships from deep-sea methane vents revealed by direct cell capture and
559 metagenomics. Proceedings of the National Academy of Sciences. 2008;105(19):7052-7.

18. Hatzenpichler R, Connon SA, Goudeau D, Malmstrom RR, Woyke T, Orphan VJ. Visualizing in situ translational activity for identifying and sorting slow-growing archaeal–bacterial consortia. Proceedings of the National Academy of Sciences. 2016;113(28):E4069-E78.

19. Schreiber L, Holler T, Knittel K, Meyerdierks A, Amann R. Identification of the dominant sulfate-reducing bacterial partner of anaerobic methanotrophs of the ANME-2 clade. Environmental Microbiology. 2010;12(8):2327-40.

20. Skennerton CT, Chourey K, Iyer R, Hettich RL, Tyson GW, Orphan VJ. Methane-fueled syntrophy through extracellular electron transfer: uncovering the genomic traits conserved within diverse bacterial partners of anaerobic methanotrophic archaea. MBio. 2017;8(4):e00530-17.

21. Holler T, Widdel F, Knittel K, Amann R, Kellermann MY, Hinrichs K-U, et al. Thermophilic anaerobic oxidation of methane by marine microbial consortia. The ISME journal. 2011;5(12):1946.

22. Niemann H, Lösekann T, De Beer D, Elvert M, Nadalig T, Knittel K, et al. Novel microbial communities of the Haakon Mosby mud volcano and their role as a methane sink. Nature. 2006;443(7113):854.

23. Su GY, Zopfi J, Yao HY, Steinle L, Niemann H, Lehmann MF. Manganese/iron-supported sulfate-dependent anaerobic oxidation of methane by archaea in lake sediments. Limnol Oceanogr. 2019.

24. Arshad A, Speth DR, de Graaf RM, den Camp HJO, Jetten MS, Welte CU. A Metagenomics-Based Metabolic Model of Nitrate-Dependent Anaerobic Oxidation of Methane by Methanoperedens-Like Archaea. Frontiers in Microbiology. 2015;6.

25. Lu Y-Z, Fu L, Ding J, Ding Z-W, Li N, Zeng RJ. Cr (VI) reduction coupled with anaerobic oxidation of methane in a laboratory reactor. Water Research. 2016;102:445-52.

585 26. Luo J-H, Chen H, Hu S, Cai C, Yuan Z, Guo J. Microbial selenate reduction driven by
586 a denitrifying anaerobic methane oxidation biofilm. Environmental Science and Technology.
587 2018;52(7):4006-12.
588 27. Shen LD, Ouyang L, Zhu YZ, Trimmer M. Active pathways of anaerobic methane
589 oxidation across contrasting riverbeds. Isme Journal. 2019;13(3):752-66.
590 28. Berger S, Frank J, Martins PD, Jetten MS, Welte CU. High-quality draft genome
591 sequence of "Candidatus Methanoperedens sp." strain BLZ2, a nitrate-reducing anaerobic
592 methane-oxidizing archaeon enriched in an anoxic bioreactor. Genome Announcements.
593 2017;5(46):e01159-17.
594 29. Ino K, Hernsdorf AW, Konno U, Kouduka M, Yanagawa K, Kato S, et al. Ecological
595 and genomic profiling of anaerobic methane-oxidizing archaea in a deep granitic
596 environment. The ISME journal. 2017;12(1):31.
597 30. Hernsdorf AW, Amano Y, Miyakawa K, Ise K, Suzuki Y, Anantharaman K, et al.
598 Potential for microbial H 2 and metal transformations associated with novel bacteria and
599 archaea in deep terrestrial subsurface sediments. The ISME journal. 2017;11(8):1915.
600 31. Vaksmaa A, Lüke C, Van Alen T, Vale G, Lupotto E, Jetten M, et al. Distribution and
601 activity of the anaerobic methanotrophic community in a nitrogen-fertilized Italian paddy
602 soil. FEMS Microbiology Ecology. 2016;92(12).
603 32. Boyd JA, Woodcroft BJ, Tyson GW. GraftM: a tool for scalable, phylogenetically
604 informed classification of genes within metagenomes. Nucleic Acids Research. 2018.
605 33. Parks DH, Imelfort M, Skennerton CT, Hugenholtz P, Tyson GW. CheckM: assessing
606 the quality of microbial genomes recovered from isolates, single cells, and metagenomes.
607 Genome research. 2015;25(7):1043-55.

608 34. Parks DH, Chuvochina M, Waite DW, Rinke C, Skarshewski A, Chaumeil P-A, et al.
609 A standardized bacterial taxonomy based on genome phylogeny substantially revises the tree
610 of life. Nature biotechnology. 2018.
611 35. Konstantinidis KT, Tiedje JM. Towards a genome-based taxonomy for prokaryotes.
612 Journal of Bacteriology. 2005;187(18):6258-64.
613 36. Thauer RK, Jungermann K, Decker K. Energy conservation in chemotrophic
614 anaerobic bacteria. Bacteriological Reviews. 1977;41(1):100.
615 37. Nauhaus K, Treude T, Boetius A, Kruger M. Environmental regulation of the
616 anaerobic oxidation of methane: a comparison of ANME-I and ANME-II communities.
617 Environ Microbiol. 2005;7(1):98-106.
618 38. Meyerdierks A, Kube M, Kostadinov I, Teeling H, Glockner FO, Reinhardt R, et al.
619 Metagenome and mRNA expression analyses of anaerobic methanotrophic archaea of the
620 ANME-1 group. Environ Microbiol. 2010;12(2):422-39.
621 39. Loach PA. Oxidation-reduction potentials, absorbance bands and molar absorbance of
622 compounds used in biochemical studies. Handbook of Biochemistry and Molecular Biology.
623 1976;1:122-30.
624 40. Jungbluth SP, Amend JP, Rappé MS. Metagenome sequencing and 98 microbial
625 genomes from Juan de Fuca Ridge flank subsurface fluids. Scientific Data. 2017;4:170037.
626 41. Welte C, Deppenmeier U. Bioenergetics and anaerobic respiratory chains of
627 aceticlastic methanogens. Biochimica et Biophysica Acta (BBA)-Bioenergetics.
628 2014;1837(7):1130-47.
629 42. Kanai T, Matsuoka R, Beppu H, Nakajima A, Okada Y, Atomi H, et al. Distinct
630 physiological roles of the three [NiFe]-hydrogenase orthologs in the hyperthermophilic
631 archaeon Thermococcus kodakarensis. Journal of Bacteriology. 2011;193(12):3109-16.

632 43. Ma K, Schicho RN, Kelly RM, Adams M. Hydrogenase of the hyperthermophile
633 Pyrococcus furiosus is an elemental sulfur reductase or sulfhydrogenase: evidence for a
634 sulfur-reducing hydrogenase ancestor. Proceedings of the National Academy of Sciences.
635 1993;90(11):5341-4.
636 44. Berney M, Greening C, Hards K, Collins D, Cook GM. Three different [NiFe]
637 hydrogenases confer metabolic flexibility in the obligate aerobe Mycobacterium smegmatis.
638 Environmental Microbiology. 2014;16(1):318-30.
639 45. Stanley EH, Casson NJ, Christel ST, Crawford JT, Loken LC, Oliver SK. The
640 ecology of methane in streams and rivers: patterns, controls, and global significance. Ecol
641 Monogr. 2016;86(2):146-71.
642 46. Deppenmeier U, Blaut M, Mahlmann A, Gottschalk G. Reduced coenzyme F420:
643 heterodisulfide oxidoreductase, a proton-translocating redox system in methanogenic
644 bacteria. Proceedings of the National Academy of Sciences. 1990;87(23):9449-53.
645 47. Timmers PH, Welte CU, Koehorst JJ, Plugge CM, Jetten MS, Stams AJ. Reverse
646 methanogenesis and respiration in methanotrophic archaea. Archaea. 2017;2017:1654237.
647 48. Walsh C. Naturally occurring 5-deazaflavin coenzymes: biological redox roles.
648 Accounts of Chemical Research. 1986;19(7):216-21.
649 49. Tran QH, Unden G. Changes in the proton potential and the cellular energetics of
650 Escherichia coli during growth by aerobic and anaerobic respiration or by fermentation.
651 European Journal of Biochemistry. 1998;251(1-2):538-43.
652 50. Tietze M, Beuchle A, Lamla I, Orth N, Dehler M, Greiner G, et al. Redox potentials
653 of methanophenazine and CoB-S-S-CoM, factors involved in electron transport in
654 methanogenic archaea. Chembiochem. 2003;4(4):333-5.

655 51. Gonzalez O, Gronau S, Pfeiffer F, Mendoza E, Zimmer R, Oesterhelt D. Systems
656 analysis of bioenergetics and growth of the extreme halophile Halobacterium salinarum.
657 PLoS Comput Biol. 2009;5(4):e1000332.
658 52. Jones AJ, Blaza JN, Varghese F, Hirst J. Respiratory complex I in Bos taurus and
659 Paracoccus denitrificans pumps four protons across the membrane for every NADH oxidized.
660 Journal of Biological Chemistry. 2017;12:4987-95.
661 53. Sazanov LA. A giant molecular proton pump: structure and mechanism of respiratory
662 complex I. Nature Reviews Molecular Cell Biology. 2015;16(6):375.
663 54. Dombrowski N, Seitz KW, Teske AP, Baker BJ. Genomic insights into potential
664 interdependencies in microbial hydrocarbon and nutrient cycling in hydrothermal sediments.
665 Microbiome. 2017;5(1):106.
666 55. Borrel G, Adam PS, McKay LJ, Chen L-X, Sierra-García IN, Sieber CM, et al. Wide
667 diversity of methane and short-chain alkane metabolisms in uncultured archaea. Nature
668 Microbiology. 2019:1.
669 56. Wang FP, Zhang Y, Chen Y, He Y, Qi J, Hinrichs KU, et al. Methanotrophic archaea
670 possessing diverging methane-oxidizing and electron-transporting pathways. ISME J.
671 2014;8(5):1069-78.
672 57. Schlegel K, Muller V. Evolution of Na and H bioenergetics in methanogenic archaea.
673 Biochem Soc Trans. 2013;41:421-6.
674 58. Schlegel K, Welte C, Deppenmeier U, Müller V. Electron transport during aceticlastic
675 methanogenesis by M ethanosarcina acetivorans involves a sodium-translocating R nf
676 complex. The FEBS journal. 2012;279(24):4444-52.
677 59. Welte C, Deppenmeier U. Membrane-bound electron transport in Methanosaeta
678 thermophila. Journal of Bacteriology. 2011;193(11):2868-70.

679 60. Anderson I, Risso C, Holmes D, Lucas S, Copeland A, Lapidus A, et al. Complete
680 genome sequence of Ferroglobus placidus AEDII12DO. Standards in genomic sciences.
681 2011;5(1):50.
682 61. Butler JE, Young ND, Lovley DR. Evolution of electron transfer out of the cell:
683 comparative genomics of six Geobacter genomes. BMC Genomics. 2010;11(1):40.
684 62. Mardanov AV, Slododkina GB, Slobodkin AI, Beletsky AV, Gavrilov SN, Kublanov
685 IV, et al. The Geoglobus acetivorans genome: Fe (III) reduction, acetate utilization,
686 autotrophic growth, and degradation of aromatic compounds in a hyperthermophilic
687 archaeon. Applied and environmental microbiology. 2015;81(3):1003-12.
688 63. Straub KL, Schink B. Ferrihydrite reduction by Geobacter species is stimulated by
689 secondary bacteria. Archives of Microbiology. 2004;182(2-3):175-81.
690 64. Levar CE, Hoffman CL, Dunshee AJ, Toner BM, Bond DR. Redox potential as a
691 master variable controlling pathways of metal reduction by Geobacter sulfurreducens. The
692 ISME Journal. 2017;11:741-52.
693 65. Vaksmaa A, Guerrero-Cruz S, van Alen TA, Cremers G, Ettwig KF, Lüke C, et al.
694 Enrichment of anaerobic nitrate-dependent methanotrophic 'Candidatus Methanoperedens
695 nitroreducens' archaea from an Italian paddy field soil. Applied Microbiology and
696 Biotechnology. 2017;101(18):7075-84.
697 66. Guiral M, Tron P, Aubert C, Gloter A, Iobbi-Nivol C, Giudici-Orticoni M-T. A
698 membrane-bound multienzyme, hydrogen-oxidizing, and sulfur-reducing complex from the
699 hyperthermophilic bacterium Aquifex aeolicus. Journal of Biological Chemistry.
700 2005;280(51):42004-15.
701 67. Vigneron A, Alsop EB, Cruaud P, Philibert G, King B, Baksmaty L, et al. Contrasting
702 Pathways for Anaerobic Methane Oxidation in Gulf of Mexico Cold Seep Sediments.
703 Msystems. 2019;4(1).

68. Yu H, Susanti D, McGlynn SE, Skennerton CT, Chourey K, Iyer R, et al. Comparative Genomics and Proteomic Analysis of Assimilatory Sulfate Reduction Pathways in Anaerobic Methanotrophic Archaea. Frontiers in Microbiology. 2018;9.

69. Zargar K, Conrad A, Bernick DL, Lowe TM, Stolc V, Hoeft S, et al. ArxA, a new clade of arsenite oxidase within the DMSO reductase family of molybdenum oxidoreductases. Environmental Microbiology. 2012;14(7):1635-45.

70. Takami H, Noguchi H, Takaki Y, Uchiyama I, Toyoda A, Nishi S, et al. A deeply branching thermophilic bacterium with an ancient acetyl-CoA pathway dominates a subsurface ecosystem. Plos One. 2012;7(1):e30559.

71. Nordstrom DK. Worldwide occurrences of arsenic in ground water. Science. 2002;296:2143-5.

72. Smedley PL, Kinniburgh D. A review of the source, behaviour and distribution of arsenic in natural waters. Applied Geochemistry. 2002;17(5):517-68.

73. Council NR. Arsenic in drinking water: National Academies Press; 1999.

74. Harvey CF, Swartz CH, Badruzzaman ABM, Keon-Blute N, Yu W, Ali MA, et al. Arsenic mobility and groundwater extraction in Bangladesh. Science. 2002;298(5598):1602-6.

75. Polizzotto ML, Harvey CF, Sutton SR, Fendorf S. Processes conducive to the release and transport of arsenic into aquifers of Bangladesh. P Natl Acad Sci USA. 2005;102(52):18819-23.

76. Anantharaman K, Brown CT, Hug LA, Sharon I, Castelle CJ, Probst AJ, et al. Thousands of microbial genomes shed light on interconnected biogeochemical processes in an aquifer system. Nature Communications. 2016;7:13219.

77. Gori F, Tringe SG, Kartal B, Machiori E, Jetten MS. The metagenomic basis of anammox metabolism in Candidatus 'Brocadia fulgida'. Biochem Soc Trans. 2011;39:1799-804.

78. Kletzin A, Heimerl T, Flechsler J, van Niftrik L, Rachel R, Klingl A. Cytochromes c in Archaea: distribution, maturation, cell architecture, and the special case of Ignicoccus hospitalis. Frontiers in microbiology. 2015;6:439.

79. Methe B, Nelson KE, Eisen JA, Paulsen IT, Nelson W, Heidelberg J, et al. Genome of Geobacter sulfurreducens: metal reduction in subsurface environments. Science. 2003;302(5652):1967-9.

80. Heidelberg JF, Paulsen IT, Nelson KE, Gaidos EJ, Nelson WC, Read TD, et al. Genome sequence of the dissimilatory metal ion–reducing bacterium Shewanella oneidensis. Nature Biotechnology. 2002;20(11):1118.

81. Slobodkina G, Reysenbach A-L, Panteleeva A, Kostrikina N, Wagner I, Bonch-Osmolovskaya E, et al. Deferrisoma camini gen. nov., sp. nov., a moderately thermophilic, dissimilatory iron (III)-reducing bacterium from a deep-sea hydrothermal vent that forms a distinct phylogenetic branch in the Deltaproteobacteria. International Journal of Systematic Evolutionary Microbiology. 2012;62(10):2463-8.

82. Ishii Si, Suzuki S, Tenney A, Nealson KH, Bretschger O. Comparative metatranscriptomics reveals extracellular electron transfer pathways conferring microbial adaptivity to surface redox potential changes. The ISME journal. 2018;12(12):2844.

83. Cochrane G, Karsch-Mizrachi I, Takagi T, Sequence Database Collaboration IN. The international nucleotide sequence database collaboration. Nucleic Acids Research. 2015;44(D1):D48-D50.

84. Li Y-L, Weng J-C, Hsiao C-C, Chou M-T, Tseng C-W, Hung J-H, editors. PEAT: an intelligent and efficient paired-end sequencing adapter trimming algorithm. BMC Bioinformatics; 2015: BioMed Central.

85. Nurk S, Meleshko D, Korobeynikov A, Pevzner PA. metaSPAdes: a new versatile metagenomic assembler. Genome Research. 2017:gr. 213959.116.

86. Seemann T. Prokka: rapid prokaryotic genome annotation. Bioinformatics. 2014;30(14):2068-9.

87. Suzek BE, Huang H, McGarvey P, Mazumder R, Wu CH. UniRef: comprehensive and non-redundant UniProt reference clusters. Bioinformatics. 2007;23(10):1282-8.

88. Tatusov RL, Fedorova ND, Jackson JD, Jacobs AR, Kiryutin B, Koonin EV, et al. The COG database: an updated version includes eukaryotes. BMC Bioinformatics. 2003;4(1):41.

89. Finn RD, Coggill P, Eberhardt RY, Eddy SR, Mistry J, Mitchell AL, et al. The Pfam protein families database: towards a more sustainable future. Nucleic Acids Research. 2016;44(D1):D279-D85.

90. Haft DH, Selengut JD, Richter RA, Harkins D, Basu MK, Beck E. TIGRFAMs and genome properties in 2013. Nucleic Acids Research. 2013;41(D1):D387-D95.

91. Burns JL, Ginn BR, Bates DJ, Dublin SN, Taylor JV, Apkarian RP, et al. Outer membrane-associated serine protease involved in adhesion of Shewanella oneidensis to Fe (III) oxides. Environ Sci Technol. 2009;44(1):68-73.

92. Marchler-Bauer A, Bryant SH. CD-Search: protein domain annotations on the fly. Nucleic Acids Research. 2004;32(suppl 2):W327-W31.

93. Yu NY, Wagner JR, Laird MR, Melli G, Rey S, Lo R, et al. PSORTb 3.0: improved protein subcellular localization prediction with refined localization subcategories and predictive capabilities for all prokaryotes. Bioinformatics. 2010;26(13):1608-15.

775 94. Bagos PG, Nikolaou EP, Liakopoulos TD, Tsirigos KD. Combined prediction of Tat
776 and Sec signal peptides with hidden Markov models. Bioinformatics. 2010;26(22):2811-7.
777 95. Eddy SR. Accelerated profile HMM searches. PLoS Comput Biol.
778 2011;7(10):e1002195.
779 96. Bateman A, Coin L, Durbin R, Finn RD, Hollich V, Griffiths-Jones S, et al. The Pfam
780 protein families database. Nucleic Acids Research. 2004;32(suppl 1):D138-D41.
781 97. Price MN, Dehal PS, Arkin AP. FastTree 2–approximately maximum-likelihood trees
782 for large alignments. Plos One. 2010;5(3):e9490.
783 98. Ludwig W, Strunk O, Westram R, Richter L, Meier H, Buchner A, et al. ARB: a
784 software environment for sequence data. Nucleic Acids Research. 2004;32(4):1363-71.
785 99. Nawrocki EP, Kolbe DL, Eddy SR. Infernal 1.0: inference of RNA alignments.
786 Bioinformatics. 2009;25(10):1335-7.
787 100. Emms DM, Kelly S. OrthoFinder: solving fundamental biases in whole genome
788 comparisons dramatically improves orthogroup inference accuracy. Genome biology.
789 2015;16(1):157.
790 101. Kolde R, Kolde MR. Package 'pheatmap'. R Package. 2015;1(7).
791 102. Greening C, Biswas A, Carere CR, Jackson CJ, Taylor MC, Stott MB, et al. Genomic
792 and metagenomic surveys of hydrogenase distribution indicate H 2 is a widely utilised energy
793 source for microbial growth and survival. The ISME journal. 2016;10(3):761.
794 103. Katoh K, Standley DM. MAFFT multiple sequence alignment software version 7:
795 improvements in performance and usability. Molecular Biology and Evolution.
796 2013;30(4):772-80.
797 104. Stamatakis A. RAxML version 8: a tool for phylogenetic analysis and post-analysis of
798 large phylogenies. Bioinformatics. 2014;30(9):1312-3.

799 105. Letunic I, Bork P. Interactive tree of life (iTOL) v3: an online tool for the display and
800 annotation of phylogenetic and other trees. Nucleic Acids Research. 2016;44(W1):W242-W5.

801

802 # Tables and Figures

803 **Table 1. Characteristics of the metagenome-assembled genomes.**
804

Bin Id	Genome size (Mbp)	No. scaffolds	N50 (scaffolds; bp)	Strain heterogeneity[#]	Compl. (%)[#]	Cont. (%)[#]	GC	#CDS	Environment	Accession no.*	16S rRNA gene?
ASW-1	1.52	271	7,386	0.0	87.5	0.0	47.8	1946	Arsenic contaminated groundwater (Bangladesh)	SRR1563167, SRR1564103, SRR1573565, SRR1573578, SAMN10961276	N
ASW-2	2.63	157	28,058	25.0	94.4	4.8	48.0	2944	Arsenic contaminated groundwater (Bangladesh)	SRR1563167, SRR1564103, SRR1573565, SRR1573578, SAMN10961277	N
ASW-3	2.51	100	44,967	0.0	100.0	1.3	50.7	2892	Arsenic contaminated groundwater (Bangladesh)	SRR1563167, SRR1564103, SRR1573565, SRR1573578, SAMN10961278	N
ASW-4	2.24	155	24,336	0.0	97.1	0.7	43.2	2464	Arsenic contaminated groundwater (Bangladesh)	SRR1563167, SRR1564103, SRR1573565, SRR1573578, SAMN10961279	N
ASW-5	2.97	221	19,046	0.0	95.0	2.6	48.9	3353	Arsenic contaminated groundwater (Bangladesh)	SRR1563167, SRR1564103, SRR1573565, SRR1573578, SAMN10961280	N
ASW-6	2.19	68	56,691	66.7	99.4	2.0	46.6	2472	Arsenic contaminated groundwater (Bangladesh)	SRR1563167, SRR1564103, SRR1573565, SRR1573578, SAMN10961281	Y

BLZ1**	3.74	514	17,508	13.33	96.73	6.56	40.2	4659	AOM-nitrate reactor (Netherlands)	LKCM00000000.1	Y
BLZ2	3.74	85	74,304	0.0	99.4	4.6	40.3	4041	AOM-nitrate reactor (Netherlands)	GCA_002487355.1	N
CMD-1	1.85	116	27,949	100.0	98.0	0.7	44.9	2261	Copper mine tailings dam (Brazil)	SRR5161805, SRR5161795, SAMN10961282	N
CMD-2	1.45	221	9,704	0.0	88.4	0.0	44.1	1786	Copper mine tailings dam (Brazil)	SRR5161805, SRR5161795, SAMN10961283	N
HGW-1	2.00	128	24,496	33.3	96.4	2.0	43.2	2288	Groundwater samples (Japan)	GCA_002839545.1	Y
IPS-1	3.52	250	27,331	10.0	97.7	5.9	44.1	3970	Paddy field soil (Italy)	GCA_900196725.1	Y
M.Ferri	2.91	59	88,069	0.0	98.7	1.3	40.8	3019	AOM-iron reactor (Australia)	GCA_003104905.1	Y
M.Nitro	3.20	10	54,4976	0.0	99.7	1.3	43.2	3428	AOM-nitrate reactor (Australia)	GCA_000685155.1	Y
MGW-1	2.08	161	17,186	0.0	97.4	3.6	44.8	2488	Groundwater samples (Japan)	Not available[§]	N
Mn-1	3.59	68	87,551	0.0	100.0	1.3	40.6	3737	AOM-manganese reactor* (Australia)	SAMN10872768	N
Mn-2	3.32	116	49,809	0.0	99.4	4.6	42.9	3684	AOM-manganese reactor* (Australia)	SAMN10872769	N

[#]Completeness (compl.), contamination (cont.), and strain heterogeneity were estimated using CheckM (33)

*Genome accession numbers. For the MAGs assembled in this study the SRA accession numbers are also given.

**The BLZ1 genome was not used in analyses as it is almost identical to the BLZ2 genome (99.5% ANI) and has inferior completeness and contamination values. The BLZ1 bioreactor was the parent system of the BLZ2 bioreactor.

§This genome was provided by Dr Yohey Suzuki and is associated with the study of Hernsdorf and colleagues (29)

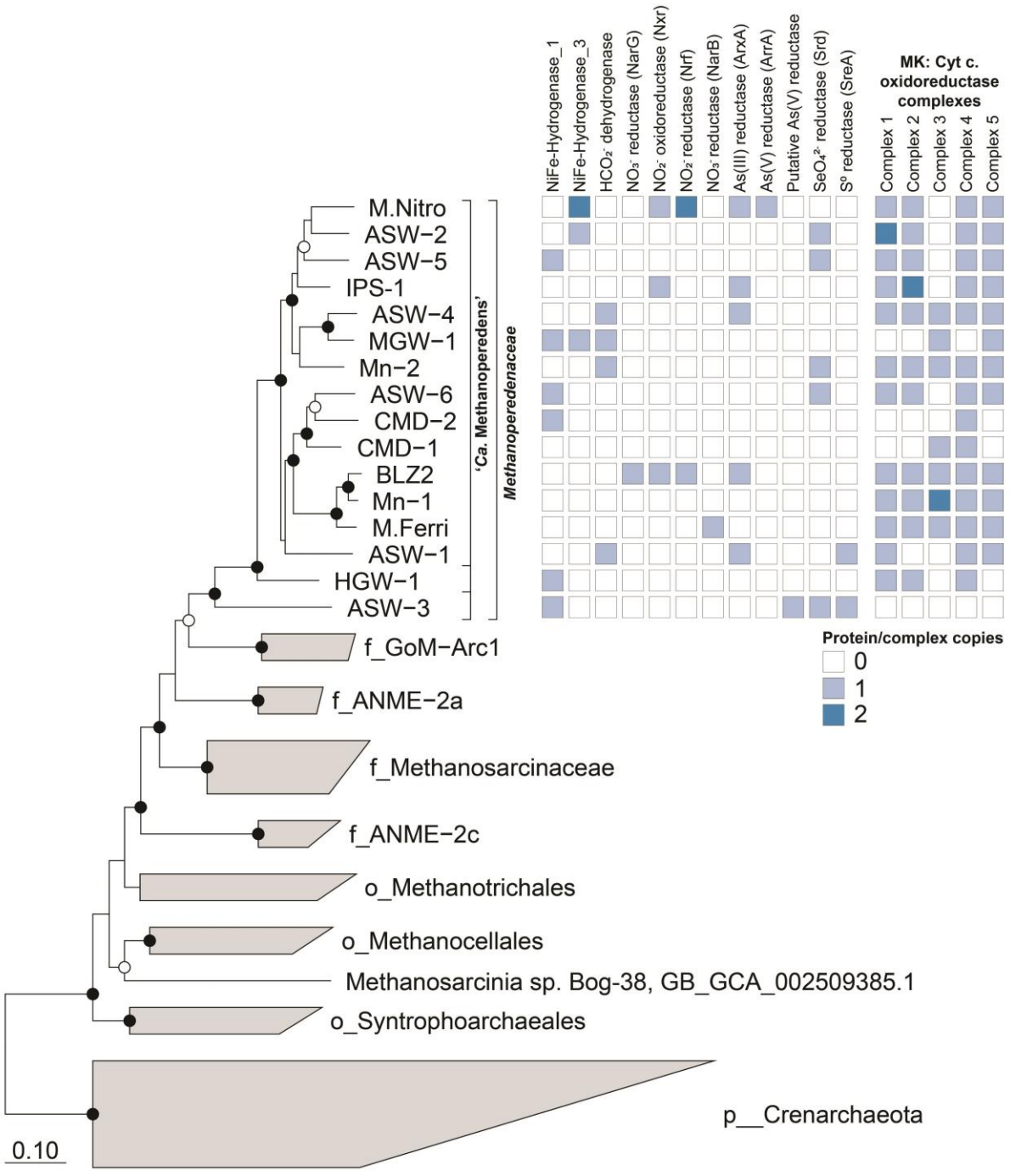

Figure 1. Phylogenetic placement of the *Methanoperedenaceae* MAGs and distribution of potential terminal electron acceptors. The genome tree was inferred using maximum-likelihood with a concatenated set of 122 archaeal specific marker genes. Black and white dots indicate >90% and >70% bootstrap values, respectively. The scale bar represents amino acids nucleotide changes. Based on GTDB-Tk the family *Methanoperedenaceae* includes

three genera including "*Ca.* Methanoperedens" which are denoted with brackets. The table to the right of the tree shows the presence/absence of gene associated with potential terminal electron acceptors in each corresponding *Methanoperedenaceae* genome.

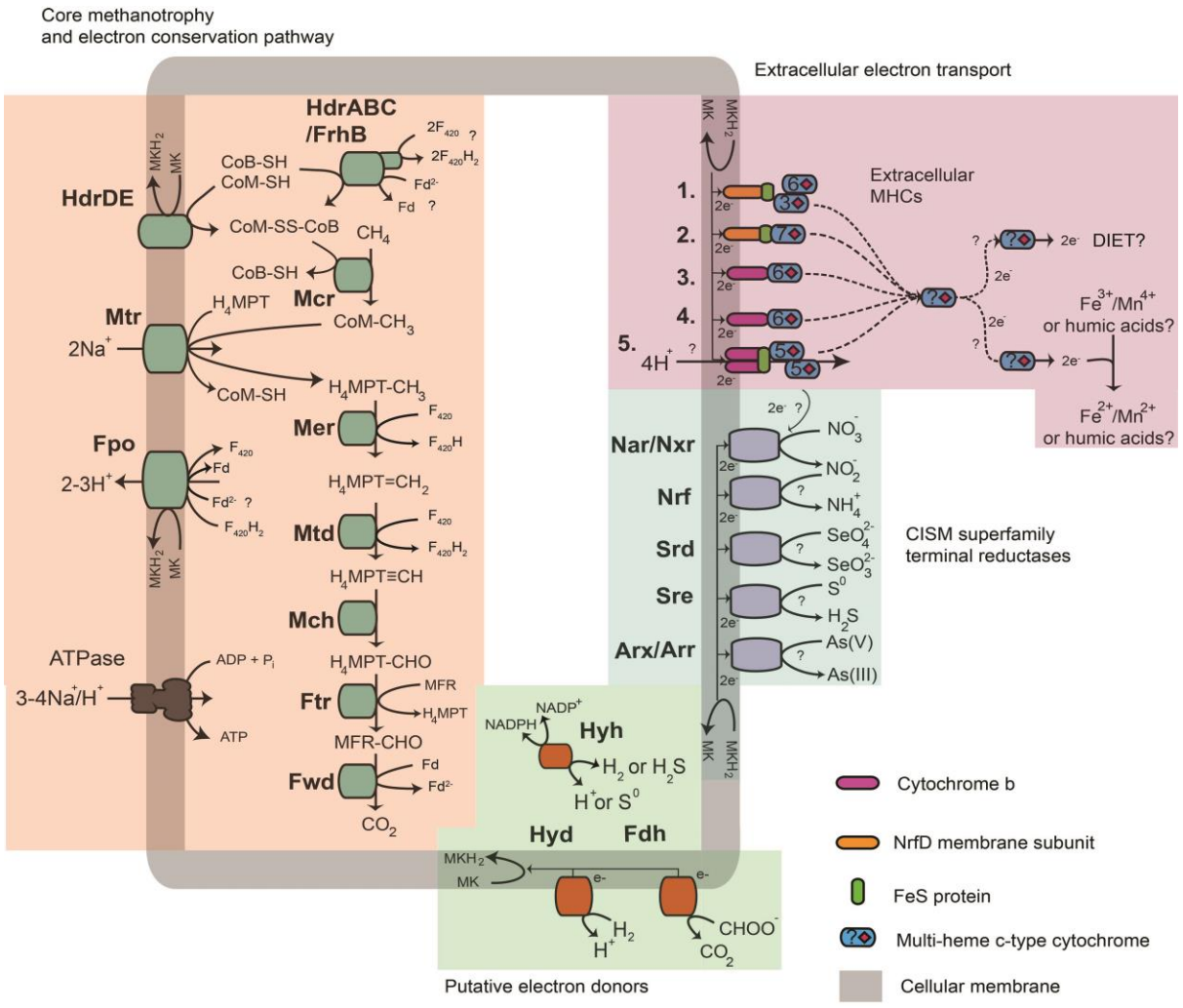

821

822 **Figure 2. Metabolic capabilities of the *Methanoperedenaceae*.** Key metabolic pathways for
823 anaerobic oxidation of methane, energy conservation mechanisms, hydrogen and formate
824 oxidation, and electron acceptors found within the pangenome of the *Methanoperedenaceae*.
825 Numbers 1-5 indicate the different menaquinone:cytochrome c oxidoreductases conserved in
826 the *Methanoperedeneceae* MAGs (**Dataset S1A**). Abbreviations for enzymes and co-factors
827 in the figure are:H_4MPT, tetrahydromethanopterin; MFR, methanofuran; Fwd, formyl-
828 methanofuran dehydrogenase; Ftr, Formylmethanofuran/H_4MPT formyltransferase; Mch,
829 methenyl-H_4MPT cyclohydrolase; Mtd, F_{420}-dependent methylene H4MPT dehydrogenase;
830 Mer, F_{420}-dependent methylene-H_4MPT reductase; Mtr, Na^+-translocating methyl-
831 H_4MPT:coenzyme M methyltransferase; Mcr, methyl-coenzyme M reductase; F_{420}, F_{420}
832 coenzyme; Fd, ferredoxin; CoM-SH, coenzyme M; CoB-HS, coenzyme B; Hdr,

heterodisulfide reductase; Fpo, $F_{420}H_2$ dehydrogenase; Hyd, type-1 NiFe hydrogenase; Hyh, type-3b NiFe hydrogenase; Fdh, formate dehydrogenase; Nar, nitrate reductase; Nrf, nitrite reductase, Ttr, tetrathionate reductase; Arx, arsenite oxidase; Arr, arsenate reductase; DIET,direct interspecies electron transfer.

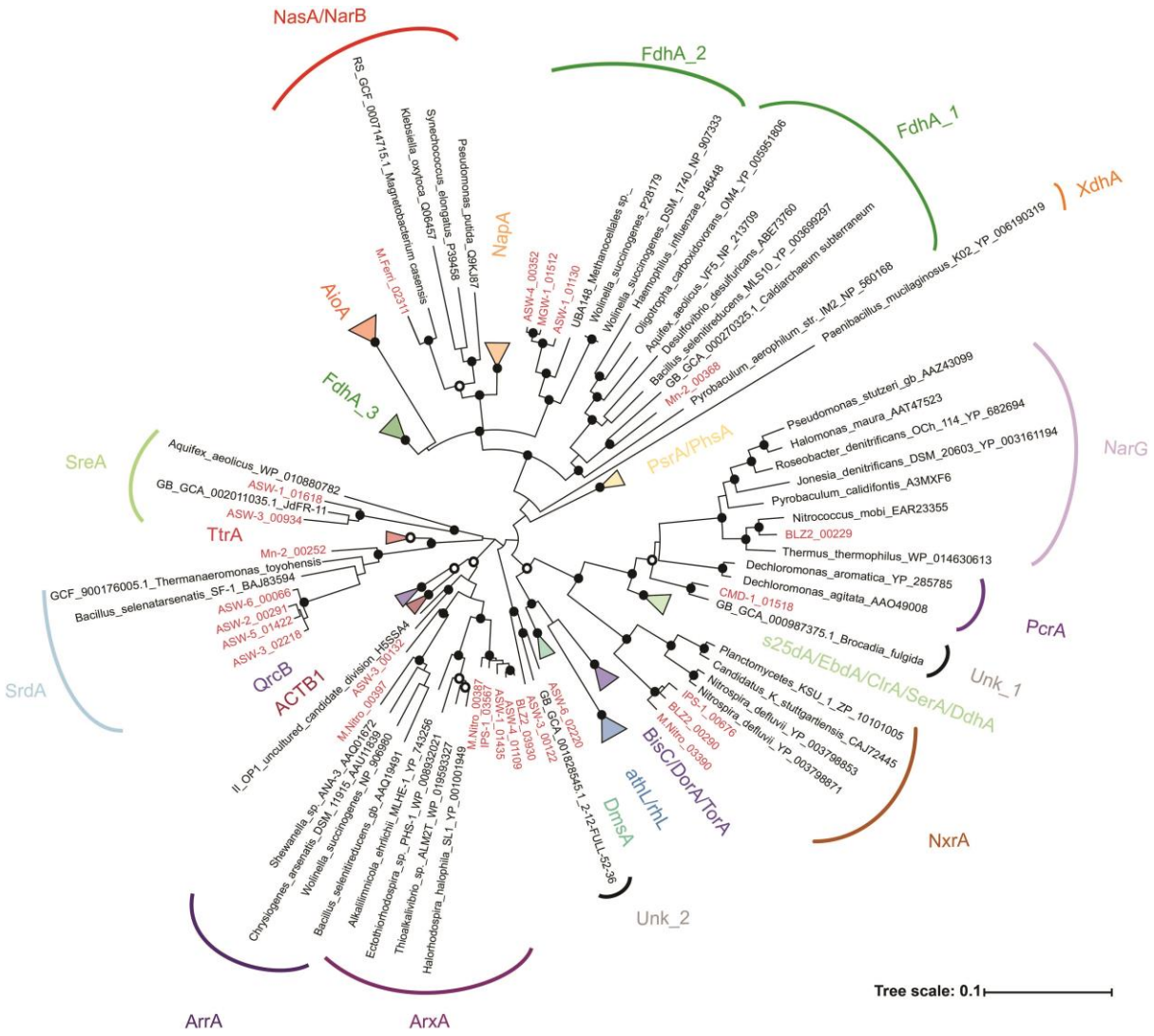

Figure 3. Phylogenetic analysis of the catalytic subunits of the CISM superfamily.

Putative genes recovered from the *Methanoperedenaceae* are highlighted in red. The gene tree was inferred by maximum-likelihood and support values calculated via non-parametric bootstrapping. Black and white dots indicate >90% and >70% bootstrap support, respectively. The scale bar represents amino acid changes. ACTB1, alternate complex III, domain of subunit B; ArrA, arsenate reductase; ArxA, arsenite oxidase; AthL, Pyrogallol hydroxytransferase; BisC, biotin sulfoxide reductase; ClrA, chlorate reductase; EbdA, Ethylbenzene dehydrogenase; s25dA, C25dehydrogenase; DmsA, DMSO reductase; DorA, DMSO reductase; NapA, nitrate reductase; NarG, nitrate reductase; NasA, assimilatory nitrate reductase; NarB, assimilatory nitrate reductase; NxrA, nitrite oxidoreductase; PsrA,

849 polysulfide reductase; PhsA, thiosulfate reductase; QrcB, quinone reductase complex; TtrA
850 tetrathionate reductase; DmsA, PcrA, perchlorate reductase; SrdA, Selenate reductase; SreA,
851 sulfreductase; TorA, TMAO reductase; XdhA, xanthine dhydrogenase; FdhA, formate
852 dehydrogenase; rhL, Resorcinol hydroxylase; Unk, unknown putative reductase. Amino acid
853 sequences are included in **Dataset S1B**.

854

Supplemental material legends

Figure S1. Average amino acid identity (AAI%) for the *Methanoperedenaceae* genomes. AAI was calculated between each pair of genomes using CompareM.

Figure S2. 16S rRNA gene based phylogenetic placement of the *Methanoperedenaceae* MAGs. The 16S rRNA genes extracted from the *Methanoperedenaceae* MAGs from this study are highlighted in red. Support values calculated via non-parametric bootstrapping. The scale bar represents changes per nucleotide position.

Figure S3. Phylogenetic analysis of methyl-coenzyme reductase subunit A (McrA). Putative genes recovered from the *Methanoperedenaceae* are highlighted in red. The gene tree was inferred using maximum likelihood and support values calculated via non-parametric bootstrapping. The scale bar represents amino acid changes.

Figure S4. Phylogenetic analysis of the subunits of the NiFe hydrogenases annotated in the *Methanoperedenaceae* genomes. A. Analysis of the catalytic subunits of the energy-converting NiFe hydrogenases. **B.** Analysis of the *b*-type cytochrome in the Group 1 NiFe hydrogenases. Putative genes recovered from the *Methanoperedenaceae* are highlighted in red. The gene trees were inferred using maximum likelihood and support values calculated via non-parametric bootstrapping. The reference sequences of Group 1 and Group 3 NiFe hydrogenases were acquired from Greening *et al.*, (C. Greening, A. Biswas, C. R. Carere, C. J. Jackson, M. C. Taylor, M. B. Stott, G. M. Cook and S. E. Morales, ISME J 10: 761-777, 2016, https://doi.org/10.1038/ismej.2015.153) and the GTDB v83 reference sequences (D.H. Parks, M. Chuvochina, D. W. Waite, C. Rinke, A. Skarshewski, P.-A. Chaumeil and P. Hugenholtz, Nat Biotechnol 36: 996-1004, 2018, https://doi.org/10.1038/nbt.4229). The scale bars represent amino acid changes.

Figure S5. Subunit compositions of the Fpo dehydrogenase protein complexes and theoretical bioenergetics of energy metabolism in ANME-2a and *Methanoperedenaceae.* **A.** Fpo subunit components for the ANME-2a and ASW-3 genomes (top left) and the other members of the *Methanoperedenaceae* (bottom left). The utilization of different electron carriers shows greater biochemical energetic gains based on more potential proton translocation. The colours orange and green depict Methanosarcinales-like and non-Methanosarcinales-like subunits. **B.** Theoretical redox potential drop when utilizing MP (left) or MK (right) during $F420H_2$ and Fd^{2-} oxidation. This is due to differences between the membrane-bound electron carriers' redox midpoint potential (Em) of -80mV and -165mV for MK and MP, respectively (M., Tietze, A. Beuchle, I. Lamla, N. Orth, M. Dehler, G. Greiner and U. Beifuss, Chembiochem 4: 333-335, 2003, https://doi.org/10.1002/cbic.200390053; Q.H. Tran and G. Unden, Eur. J. of Biochem. 251: 538-543, 1998, https://doi.org/10.1046/j.1432-1327.1998.2510538.x).

Figure S6. Phylogenetic analysis of the Fpo subunits annotated in the *Methanoperedenaceae* genomes. A. FpoA **B.** FpoB **C.** FpoC **D.** FpoD **E.** FpoH **F.** FpoI **G.** FpoJ1 **H.** FpoJ2 **I.** FpoK **J.** FpoL **K.** FpoM **L.** FpoN **M.** FpoO. Putative genes recovered from the *Methanoperedenaceae* are highlighted in red. The gene trees were inferred using maximum likelihood and support values calculated via non-parametric bootstrapping. Reference genes and the taxonomy are from the GTDB v83 database (D.H. Parks, M. Chuvochina, D. W. Waite, C. Rinke, A. Skarshewski, P.-A. Chaumeil and P. Hugenholtz, Nat Biotechnol 36: 996-1004, 2018, https://doi.org/10.1038/nbt.4229).

Figure S7. Phylogenetic analysis of the subunits of the MK:cytochrome oxidoreductases annotated in the *Methanoperedenaceae* MAGs. A. Analysis of the NrfD subunits. **B.** Analysis of the b-type cytochromes. Bootstrap values for the maximum-likelihood trees were

902 determined using non-parametric bootstrapping with 100 replicates. The scale bars represent
903 amino acid changes.

904 **Figure S8. Abundance profiles for the MHC orthologous protein families annotated in**
905 **the *Methanoperedenaceae* MAGs.**

906 **Figure S9. Network analysis of MHC orthologous protein families in**
907 ***Methanoperedenaceae*.** Each cluster represents related MHCs. The colour of the nodes
908 represents the taxonomic lineage based on GTDB classification. The size of the nodes
909 represents the number of CXXCH heme binding motifs identified in the proteins. The
910 thickness of the lines represents amino acid identity between the two nodes. The shaded
911 boxes represent the orthologous protein families.

912 **Dataset S1. Sequences, identifiers and statistics for genes used in the comparative**
913 **analyses of the *Methanoperedenaceae* MAGs. A.** Genes encoding proteins involved in the
914 methane oxidation pathway, energy conservation, and other metabolic pathways as shown in
915 Figure 2. **B.** Amino acid sequences used in the CISM superfamily gene tree (Figure 3).
916 Amino acid sequences include curated sequences from Swiss-Prot and Castelle *et al.,* (C.J.
917 Castelle, L. A. Hug, K. C. Wrighton, B. C. Thomas, K. H. Williams, D. Wu, S. G. Tringe, S.
918 W. Singer, J. A. Eisen and J. F. Banfield, Nat commun 4: 2120, 2013,
919 https://doi.org/10.1038/ncomms3120) and closely related sequences from GTDB r83 protein
920 reference database (D.H. Parks, M. Chuvochina, D. W. Waite, C. Rinke, A. Skarshewski, P.-
921 A. Chaumeil and P. Hugenholtz, Nat Biotechnol 36: 996-1004, 2018,
922 https://doi.org/10.1038/nbt.4229). **C.** Amino acid sequences used in the catalytic subunits of
923 the energy-converting NiFe hydrogenase. Amino acid sequences include curated sequences
924 from Greening *et al.,* (C. Greening, A. Biswas, C. R. Carere, C. J. Jackson, M. C. Taylor, M.
925 B. Stott, G. M. Cook and S. E. Morales, ISME J 10: 761-777, 2016,

926 https://doi.org/10.1038/ismej.2015.153) and closely related sequences from GTDB r83
927 protein reference database. **D.** Genes encoding putative NiFe hydrogenase maturation
928 proteins. **E.** Best blastp hits of Fpo dehydrogenase subunits to the IMG database. Blastp hits
929 shows divergent Fpo subunits are present in the *Methanoperedeneceae* MAGs as seen in
930 Figure S6. Top blast hits to Methanoperedens-like protein sequences were excluded. **F.**
931 General statistic of multi-heme *c*-type cytochromes (MHCs) in the ANME genomes. **G.**
932 MHC general statistics for all bacterial and archaeal families in the GTDB v89 database.

933